


## Article

# Spatio-Temporal Changes and Influencing Factors of Meteorological Dry-Wet in Northern China during 1960–2019

Junju Zhou <sup>1,2,3</sup>, Haitao Tang <sup>1,\*</sup>, Yu Qiu <sup>1</sup>, Zhaonan Guo <sup>1</sup>, Chuyu Luo <sup>1</sup>, Xue Wang <sup>1</sup>, Wei Shi <sup>1,2</sup>, Dongxia Zhang <sup>1</sup>, Chunli Wang <sup>1</sup>, Xuemei Yang <sup>4</sup>, Chunfang Liu <sup>1,3</sup> and Wei Wei <sup>1</sup> 

<sup>1</sup> College of Geography and Environmental Science, Northwest Normal University, Lanzhou 730070, China; yzh\_su@163.com (J.Z.); 13919458450@163.com (Y.Q.); guo229478@163.com (Z.G.); xiaowo\_luo@163.com (C.L.); wangxuedoris@163.com (X.W.); shiwei@nwnu.edu.cn (W.S.); zhangdongxia@nwnu.edu.cn (D.Z.); chunliwang@nwnu.edu.cn (C.W.); liuchunfang@nwnu.edu.cn (C.L.); weiweigis2006@126.com (W.W.)

<sup>2</sup> Key Laboratory of Resource Environment and Sustainable Development of Oasis, Lanzhou 730070, China

<sup>3</sup> Gansu Engineering Research Center of Land Use and Comprehension Consolidation, Lanzhou 730070, China

<sup>4</sup> School of Tourism, Lanzhou University of Arts and Sciences, Lanzhou 730020, China; yxm9693@163.com

\* Correspondence: tht1215024616@163.com

**Abstract:** In northern China, precipitation fluctuates greatly and drought occurs frequently, which mark some of the important threats to agricultural and animal husbandry production. Understanding the meteorological dry-wet change and the evolution law of drought events in northern China has guiding significance for regional disaster prevention and mitigation. Based on the standardized precipitation index (SPI), this paper explored the spatio-temporal evolution of meteorological dry-wet in northern China. Our results showed that arid area (AA) and semi-arid area (SAA) in the west showed a trend of wetting at inter-annual and seasonal scales, while humid area (HA) and semi-humid area (SHA) in the east showed a different dry-wet changing trend at different seasons under the background of inter-annual drying. AA and HA showed obvious “reverse fluctuation” characteristics in summer. The drought frequency (DF) and drought intensity (DI) were high in the east and low in the west, and there was no significant difference in drought duration (DD) and drought severity (DS) between east and west. The DD, DS and DI of AA and SAA showed a decreasing trend, while the DD and DS of HA and SHA showed a slight increasing trend, and the DS decreased. In summer and autumn, the main influencing factors of drying in the east and wetting in the west were PNA, WP, PDO and TP1, and the fluctuations of NAO-SOI, NAO-AMO and PNA-NINO3.4 jointly determined the characteristics of SPI3 reverse fluctuations of HA and AA in summer.

**Keywords:** northern China; dry-wet change; drought evolution; SPI; teleconnection factor



**Citation:** Zhou, J.; Tang, H.; Qiu, Y.; Guo, Z.; Luo, C.; Wang, X.; Shi, W.; Zhang, D.; Wang, C.; Yang, X.; et al. Spatio-Temporal Changes and Influencing Factors of Meteorological Dry-Wet in Northern China during 1960–2019. *Sustainability* **2023**, *15*, 1499. <https://doi.org/10.3390/su15021499>

Academic Editor: Swadhin Behera

Received: 15 December 2022

Revised: 3 January 2023

Accepted: 9 January 2023

Published: 12 January 2023



**Copyright:** © 2023 by the authors. Licensee MDPI, Basel, Switzerland. This article is an open access article distributed under the terms and conditions of the Creative Commons Attribution (CC BY) license (<https://creativecommons.org/licenses/by/4.0/>).

## 1. Introduction

Drought is a natural disaster caused by a long-term water shortage [1–3], which has the characteristics of high frequency, long duration and wide impact [4–9], causing great harm to the natural ecology, social economy and human habitat [10–19]. Under the background of global warming, drought may be further aggravated [20–22]. In order to reduce the harm caused by drought as much as possible, it is significant and urgent to effectively monitor and evaluate drought [23].

In order to quantitatively study the occurrence of drought and monitor the change trend of drought [24–26], scholars have put forward various drought indices in recent years. Commonly used drought indices include the Palmer drought severity index (PDSI) [27], standardized precipitation index (SPI) [28] and standardized precipitation evapotranspiration index (SPEI) [4]. The Palmer Drought Severity Index (PDSI) comprehensively considers the influence of precipitation, temperature and the underlying surface, and has a good response to medium and long-term drought. However, its calculation is complex and only

applicable to a single time scale, which makes it difficult to accurately reflect short-term drought [29]. The standardized precipitation evapotranspiration index (SPEI) takes PET into account, but in fact in arid and semi-arid areas where potential evapotranspiration is greater than precipitation, the monthly total PET is actually the amount of water that is not available and therefore cannot be evaporated and transpired. Its use may lead to inaccurate estimates of drought events, such as overestimating droughts [30–33]. The standardized precipitation index (SPI) is a standardized value that expresses the actual precipitation as a deviation from the probability distribution function of precipitation. It is a powerful tool widely applied for drought research with the advantages of convenient calculation, multi-time scale and so on [34]. At the same time, SPI only needs to take precipitation as input data, avoiding the problem of parameter calibration and it is especially suitable for drought and flood monitoring in areas with scarce hydrological data [24]. Scholars have conducted a lot of research using SPI, including in North Africa [35], East Africa [34], Central Asia [36], East Asia [37], South America [38], the Mediterranean Sea [39,40] and areas such as the Caribbean [41]. Anyway, SPI has shown a great response to drought conditions in these areas even in the various dry-wet climate conditions.

A large number of studies have shown that the internal variability of the climate system and external forcing (natural forcing and human activities) are the main factors driving the inter-decade change of climate events, and the dry-wet change of climate is mainly influenced by the internal variability of the climate system [42]. The internal variability of the climate system is often expressed by some teleconnection factors, such as AMO, IPO, PDO, etc. [43–47]. The teleconnection factor is a strong signal generated by the interaction between ocean and atmospheric circulation during global change, which affects the exchange process of mass, momentum and heat in the atmosphere, and then causes climate anomaly [48]. Previous studies have shown that the changes of teleconnection factors had a profound impact on regional dry-wet change or drought evolution. For example, the changes in precipitation and runoff in Alberta, Ontario and Newfoundland were mainly influenced by ENSO, NAO and PDO [49]; the future precipitation change in California was mainly influenced by ENSO [50]; the extreme precipitation model in Europe was closely related to AMO [51]; the evolution process of drought in arid area of China from 1960 to 2010 was mainly influenced by polar vortex, AO and NAO in the northern hemisphere, and the drought change in southern Xinjiang and Hexi Corridor might also be influenced by the Qinghai-Tibet Plateau high [52]; the inter-decade variation of humidity in the Qinghai-Tibet Plateau was mainly influenced by the PDO model [53]; the drought in the North China Plain was greatly influenced by ENSO [23]. Thus, the teleconnection factors may directly and indirectly impact the occurrence of drought, which deserve to be further investigated.

The northern regions of China span from east to west with obvious differences in precipitation. As the developed areas of the planting industry in China, the sub-humid area and humid area in the east belong to the monsoon region, which are significantly affected by the monsoon circulation with large precipitation. As the important pastoral areas in China, the semi-arid area and arid areas in the west belong to the non-monsoon region, which are mainly controlled by the westerly belt with less precipitation. Are precipitation or meteorological dry-wet fluctuations and their evolution the same in humid area and arid area under different circulation systems? What are the differences and internal relations? Up to now, these questions lack accurate answers, which has become the bottleneck of formulating differentiated water resource management and disaster prevention and mitigation policies in Northern China. Due to the complexity of the circulation systems affecting Northern China, there should be an “alternating growth and decline” phenomenon among different circulation systems. Therefore, the basic hypothesis of this paper is that the “alternating growth and decline” seesaw effect should also take place in the change trend and fluctuation process of the meteorological dry-wet in dry-wet areas located in Northern China. Based on the existing research, the evolution characteristics and influencing factors of meteorological dry-wet changes and drought events in Northern

China in the past 60 years were analyzed in this paper to explore the problems above. The evolution law, spatial heterogeneity and internal relationship of meteorological dry-wet and drought events in Northern China would be revealed at last. The specific research objectives of this paper are as follows: (1) to reveal the characteristics of dry-wet changes and drought evolution in Northern China; (2) to explore the relationship between dry-wet change and teleconnection factors in each dry-wet area; (3) to find the driving factors of dry-wet change in each dry-wet area, and to explain the driving mechanism of dry-wet changes.

## 2. Data and Methodology

### 2.1. Study Area and Data Collection

#### 2.1.1. Study Area

The research area of this paper is Northern China, north of the Huaihe-Qinling-Kunlun mountain line, located between  $73^{\circ}33' E$ – $135^{\circ}05' E$  and  $31^{\circ}23' N$ – $53^{\circ}33' N$ , covering an area of about 5.7672 million  $km^2$ , including 15 provincial administrative regions such as Heilongjiang Province and Xinjiang Uygur Autonomous Region (Figure 1) [54]. The study area is rugged and spans three steps from west to east. The landforms are diverse and complex, including deserts, mountains, hills, plateaus, plains and basins. Climate types varied, including monsoon climate, temperate continental climate and highland mountain climate. Annual precipitation drops from 1000 mm to less than 100 mm from east to west. According to the annual average precipitation, the study area can be divided into humid area, semi-humid area, semi-arid area and arid area. Greater than 800 mm is humid area (HA), 400–800 mm is semi-humid area (SHA), 200–400 mm is semi-arid area (SAA), and less than 200 mm is arid area (AA). The landscapes of the study area were forest, grassland, desert grassland and desert in order from east to west. Natural disasters in the study area, especially the frequent drought disasters, have caused great harm and loss to the ecological environment and social economy.

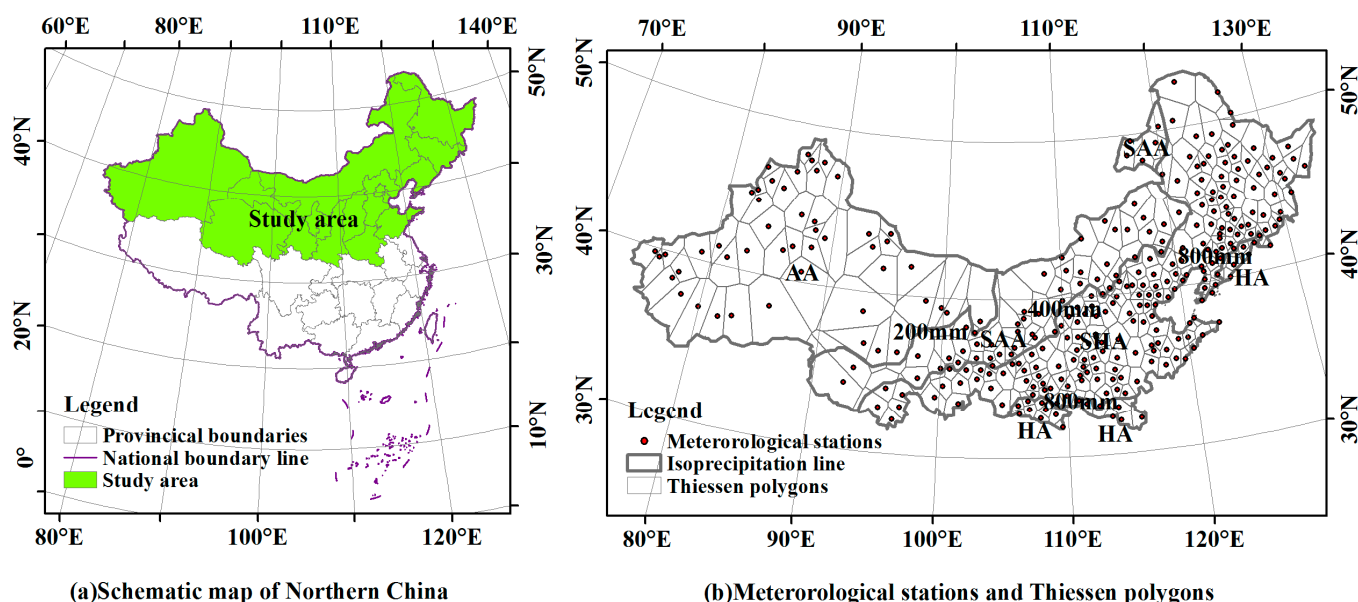


**Figure 1.** Location of the study area.

#### 2.1.2. Data Collection

The monthly precipitation series data of meteorological stations in Northern China from 1960 to 2019 came from China Meteorological Data Network (<http://data.cma.cn>, accessed on 31 October 2020). Due to a large number of missing values in the observed data, the meteorological stations were screened. These meteorological stations were removed if there were continuous missing data for more than two years in the same month or total

missing data for more than three years. For the remaining meteorological stations, the monthly precipitation would be replaced by the multi-year average of precipitation for that month of the meteorological station if there were missing values. Finally, the data from 320 eligible meteorological stations (as shown in Figure 1) were left for this study. Ocean teleconnection indices data came from the National Oceanic and Meteorological Administration (<http://www.noaa.gov/>, accessed on 31 October 2020), including Arctic Oscillation Index (AO), North Atlantic Oscillation Index (NAO), Western Pacific Oscillation Index (WP), Pacific-North America Teleconnection Index (PNA), ENSO Index (NINO3.4), Atlantic Multiannual Oscillation Index (AMO), Southern Oscillation Index (SOI), North Pacific Interdecadal Oscillation Index (PDO), etc. The data in the plateau monsoon index (TP1) and Asian polar vortex intensity index (APV) came from the National Climate Center of China Meteorological Administration (<http://cmdp.ncc.cma.gov.cn>, accessed on 31 October 2020). All index data spanned from 1960 to 2019.

## 2.2. Methodology

### 2.2.1. Thiessen Polygon

Most often, the arithmetic mean method, the Thiessen polygon method and the isohyet method are used to calculate regional average precipitation. The arithmetic mean method is suitable for areas where the meteorological stations are evenly distributed. The Thiessen polygon method is applicable for areas with uneven distribution of meteorological stations. The isohyet method is suitable for areas with a large topographic fluctuation and sufficient rainfall stations. The distribution of meteorological stations in Northern China is uneven, with dense distribution of meteorological stations in the east and sparse in the west. Different meteorological station controls different area sizes, so the Thiessen polygon method is more suitable for Northern China than the arithmetic mean method and isohyet method. The Thiessen polygon constructed in this paper was shown in Figure 1. The formula for calculating regional mean precipitation [55] is as follows:

$$\bar{P} = \sum_{i=1}^n w_i p_i = \sum_{i=1}^n \frac{S_i}{S} p_i \quad (1)$$

$\bar{P}$  is the regional mean precipitation,  $w_i$  is the Thiessen weight,  $S_i$  is the Thiessen polygon area of  $i$  weather station,  $S$  is the total area of the region, and  $P_i$  is the precipitation of  $i$  weather station.

### 2.2.2. Standardized Precipitation Index (SPI)

Precipitation distribution is a skewed distribution rather than a normal distribution. Mckee et al. [32] used Gamma probability distribution to describe the distribution changes of precipitation and then obtained SPI values after normal normalization. The calculation steps referred to Zhou Junju, Kalisa and Abdelmalek et al. [34,39,54,56,57]. Assuming that the precipitation in a certain period is  $x$ , the probability density function satisfying the Gamma distribution is

$$g(x) = \frac{1}{\beta^\alpha \Gamma(\alpha)} x^{\alpha-1} e^{-x/\beta} \quad (2)$$

where:  $\alpha$  is the shape parameter,  $\beta$  is the scale parameter, and  $x$  is the precipitation.  $\Gamma(\alpha)$  is Gamma function, and its probability function is:

$$\Gamma(\alpha) = \int_0^{\infty} y^{\alpha-1} e^{-y} dy \quad (3)$$

The best estimates of  $\alpha$  and  $\beta$  can be obtained by the maximum likelihood estimation method:

$$\hat{\alpha} = \frac{1}{4A} \left( 1 + \sqrt{1 + \frac{4A}{3}} \right) \quad (4)$$

$$\hat{\beta} = \frac{\bar{x}}{\hat{\alpha}} \quad (5)$$

$$A = \ln(\bar{x}) - \frac{\sum \ln(x_i)}{n} \quad (6)$$

where:  $x_i$  is the sample of precipitation series,  $\bar{x}$  is the average value of precipitation series, and  $n$  is the length of calculated series. Then, the cumulative probability of a given time length can be calculated by the following formula:

$$G(x) = \int_0^x g(x)dx = \frac{1}{\hat{\beta}\Gamma(\hat{\alpha})} \int_0^x x^{\hat{\alpha}-1} e^{-x/\hat{\beta}} dx \quad (7)$$

Since the Gamma equation does not include the case of  $x = 0$  and the actual precipitation may be 0, the cumulative probability is expressed as:

$$H(x) = q + (1 - q)G(x) \quad (8)$$

where:  $q$  is the probability of zero precipitation. If  $m$  is the number of precipitation events with 0 in precipitation time series, there is  $q = m/n$ .

The cumulative probability  $H(x)$  can be converted into a standard normal distribution function by the following formula:

$$H(x) = \frac{1}{\sqrt{2\pi}} \int_{-\infty}^x e^{-t^2/2} dt \quad (9)$$

The following results are obtained by approximate solution:

$$SPI = -\left(t - \frac{c_0 + c_1t + c_2t^2}{1 + d_1t + d_2t^2 + d_3t^3}\right) \quad (10)$$

$$t = \sqrt{\ln\left(\frac{1}{(H(x))^2}\right)} \quad (11)$$

where  $0.5 < H(x) \leq 1$ :

$$SPI = \left(t - \frac{c_0 + c_1t + c_2t^2}{1 + d_1t + d_2t^2 + d_3t^3}\right) \quad (12)$$

$$t = \sqrt{\ln\left(\frac{1}{(1.0 - H(x))^2}\right)} \quad (13)$$

where  $c_0 = 2.515517$ ,  $c_1 = 0.802853$ ,  $c_2 = 0.010328$ ,  $d_1 = 1.432788$ ,  $d_2 = 0.189269$ ,  $d_3 = 0.001308$ .

In this paper, SPI\_SL\_6.exe software was used to calculate the SPI1, SPI3 and SPI12. SPI3 in May, August, November and February of the next year were selected as the SPI of the four seasons (spring, summer, autumn and winter) of the year, and SPI12 in December of each year was selected as the annual SPI of the year. According to relevant studies [54,56–58] and the classification standard of National Climate Center, combined with the reality of Northern China, the classification standard of the dry-wet level is as follows (Table 1):

**Table 1.** Classification of dry or wet conditions of the SPI.

SPI Value	Categories	SPI Value	Categories
$\geq 2$	Extremely wet	−0.99 to −0.50	Mildly drought
1.50–1.99	Very wet	−1.49 to −1.0	Moderately drought
1.0–1.49	Moderately wet	−1.99 to −1.50	Very drought
0.50–0.99	Mildly wet	$\leq -2.0$	Extremely drought
−0.49–0.49	Normal		

### 2.2.3. Drought Identification

Run theory is a method to analyze time series, which is widely used in the identification of drought events [59–64]. The run theory has undergone a process of development. Most of the past studies were based on the single threshold run theory for drought event identification [59,62]. This raised the following two questions: (1) too many small droughts complicated the analysis of drought event sequence. Can they be eliminated? (2) Droughts with short intervals had temporal correlation. Can they be combined into one drought event? What were the criteria for merging? The above two problems were solved and the accuracy of drought event identification was increased after the improved run theory method proposed by He et al. [63]. Three thresholds were included in the improved run theory method: drought occurrence threshold  $X_1$ , drought elimination threshold  $X_2$  and drought combination threshold  $X_0$ . Drought can occur only with negative run, so the threshold  $X_0 = 0$  was set. According to the classification standard of SPI drought grade, mildly drought occurred when  $SPI \leq -0.5$ , so the threshold  $X_2 = -0.5$  was set. Even if the level of mild drought was not reached, the persistent lack of precipitation in an area can also have a negative impact on the socio-economic environment. Wang Xiaofeng et al. [61] also believed that drought occurred when the SPI value of two or more consecutive periods was in the range of  $-0.5$  to  $-0.3$ , so the threshold  $X_1 = -0.3$  and  $X_1 = -0.4$  were set to identify drought events. The advantage of doing so is that we can compare the effectiveness of different thresholds to identify drought events in order to select a more suitable threshold for this study. In this study, the monthly scale SPI (SPI1) was used to identify drought events, and the recognition process was as follows.

The first step was to preliminarily determine the drought events according to the threshold  $X_1$ , from which six drought events (a, b, c, d, e, f) could be pre-selected. The second step was to eliminate the drought event that lasted for one month but did not reach the threshold  $X_2$ , thus the drought event a could be eliminated. The third step was the merger. If the interval between two adjacent drought events was 1 month and the index value of the interval month was less than the threshold value  $X_0$ , the two droughts were combined into one drought, thus droughts b and c could be combined into one drought (Figure 2).

Drought frequency ( $DF$ ) was defined as the number of drought events, and drought duration ( $DD$ ) was defined as the time span (month) of a drought event. Drought severity ( $DS$ ) was the sum of the absolute values of all SPIs in a drought event, and drought intensity ( $DI$ ) was the severity of a drought event divided by the duration.



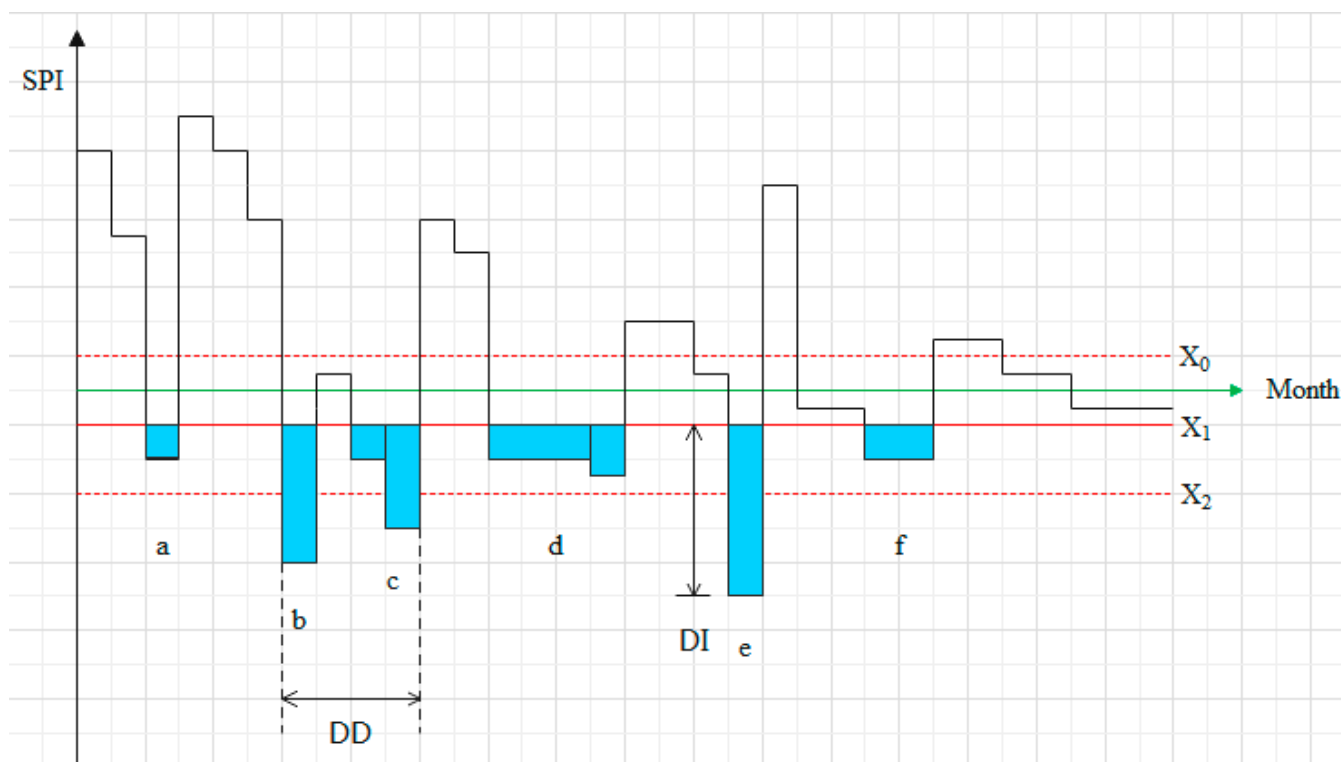


**Figure 2.** Drought event identification process.

Drought duration ( $DD$ ), drought severity ( $DS$ ) and drought intensity ( $DI$ ) are calculated as follows:

$$DD = t_s - t_e \quad (14)$$

$$DS = \sum_{i=t_s}^{t_e} |Z_i| \quad (15)$$

$$DI = \frac{DS}{DD} \quad (16)$$

$t_s$  is the start time of a drought event,  $t_e$  is the end time of a drought event,  $Z_i$  is the index value of time  $i$  within a drought event.

#### 2.2.4. Mann-Kendall Trend Test and Sen's Trend

The Mann-Kendall trend test [65,66] is a robust non-parametric statistical trend calculation method with the advantages of high computational efficiency and insensitivity to measurement error and outlier data, which is commonly used for trend analysis of long time series data [67]. It is the main method for trend judgment in the field of meteorology and hydrology [68,69]. For estimating the slope of linear trend, the application of the Sen trend degree is so necessary that it has been widely used to determine the size of the trend in hydro-meteorological time series [70–72]. In this paper, both Mann-Kendall test and Sen trend degree were used to calculate the variation trend and size of SPI of each meteorological station.

### 3. Results

#### 3.1. Dry-Wet Change Characteristics

##### 3.1.1. Characteristics of Meteorological Dry-Wet Change in Northern China

Based on the values of SPI12 and SPI3 of 320 meteorological stations in Northern China during 1960–2019, the change tendency rates were calculated, and our results were shown in Figure 3 and Table 2.

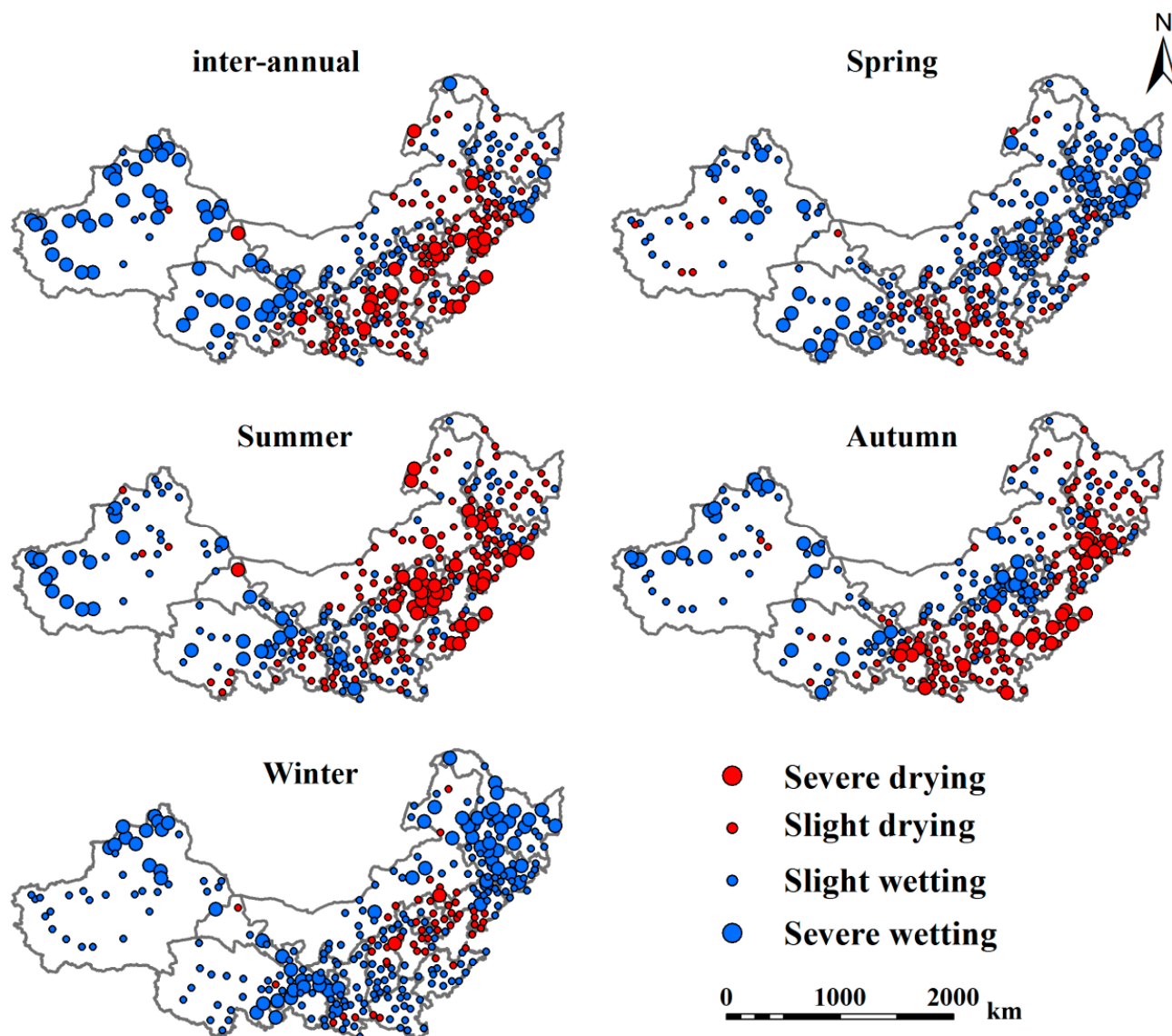


Figure 3. Tendency rates of SPI change of meteorological stations. [min,1/2 min).

Table 2. Statistics on the number of drying and wetting stations.

	Inter-Annual	Spring	Summer	Autumn	Winter
Wetting	173 (54.06%)	243 (75.94%)	138 (43.13%)	145 (45.31%)	269 (84.06%)
Drying	147 (45.94%)	77 (24.06%)	182 (56.87%)	175 (54.69%)	51 (15.94%)



[1/2 min,0), [0,1/2 max), [1/2 max,max] represents severe drying, slight drying, slight wetting, and severe wetting, respectively [29].

At the inter-annual scale, the number of stations with wetting (173) was slightly larger than that with drying (147), and the stations with wetting were mainly distributed in the arid area (AA), semi-arid area (SAA) and the northeast of the semi-humid area (SHA). In terms of seasonal scales, the number of stations with wetting in winter and spring (269 and 243, respectively) was much larger than that with drying (51 and 77, respectively). Especially in winter, the drying ones only appeared in the central part of the SHA. The number of wetting stations in summer and autumn (138 and 145, respectively) was slightly lower than that of drying stations (182 and 175, respectively), showing characteristics of humid area (HA) and SHA in the east becoming drying and SAA and AA in the west became wetting. Overall, the AA and SAA in the west had the same trend of wetting at the inter-annual and seasonal scales, while the HA and SHA in the east had complex meteorological dry-wet changes in different seasons.

### 3.1.2. Regional Differences of Meteorological Dry-Wet Changes

#### The Trend of Meteorological Dry-Wet Change in Different Seasons

As shown in Figure 4, at the inter-annual scale, the AA and SAA showed the trend of meteorological wetting. Especially in the AA, the wetting trend was the most obvious with a SPI12 change tendency rate of 0.299/10a, while the HA had the most obvious meteorological drying trend with a SPI12 change tendency of  $-0.046/10a$ . In winter, the four areas all showed the trend of meteorological wetting, and the change tendency rates from large to small were as follows: AA, SAA, SHA and HA. In spring, a weak trend of meteorological drying was observed only in the HA, and the fastest wetting speed was in the SAA. There were pronounced consistency between summer and autumn, that is, the AA and SAA were wetting, while the SHA and HA were drying.

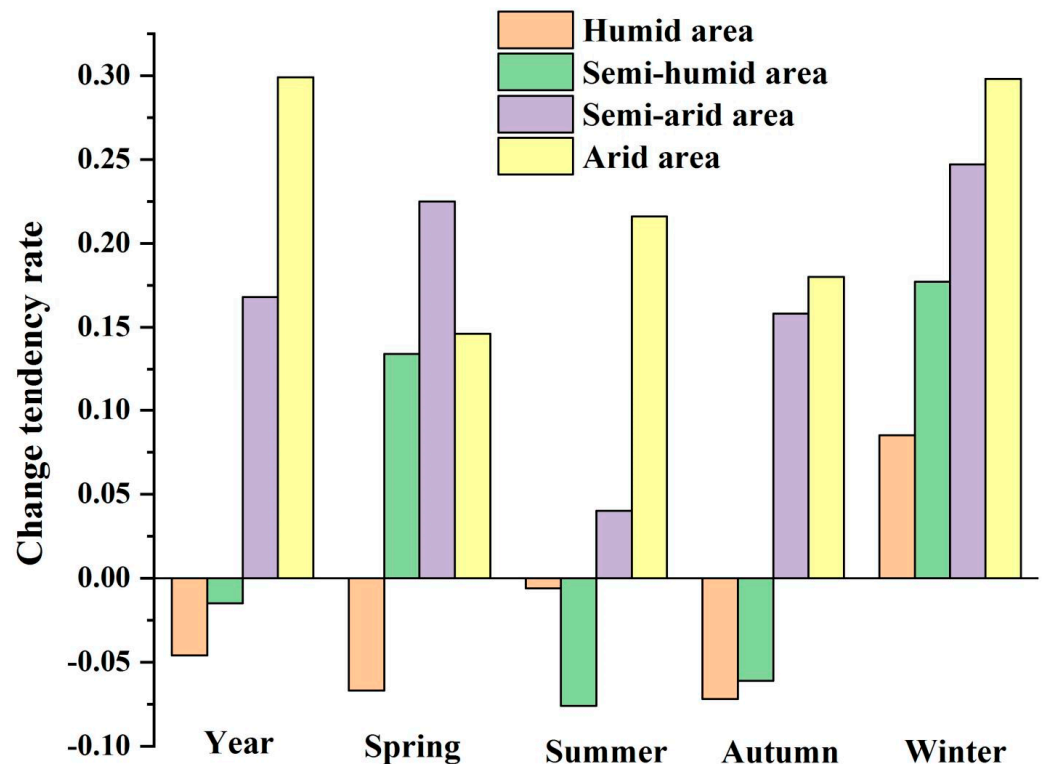


Figure 4. Tendency rates of SPI change in four areas of Northern China in different seasons.

### Analysis of Dry-Wet Fluctuation Process

In order to further analyze the fluctuating relationship in the process of meteorological dry-wet change in different dry-wet areas, the 5a moving average was carried out for SPI3 in different seasons (Figure 5). It can be found that there was an obvious reverse fluctuation process (seesaw effect) in SPI3 in AA and HA in summer. The obvious reverse fluctuation process of SPI3 also appeared in HA and SAA from the 1970s to 2010, while SHA and AA had obvious reverse fluctuation characteristics in SPI3 before the 1990s. However, in autumn, winter and spring, SPI3 in the four regions showed a “simultaneously and reverse” fluctuation process.

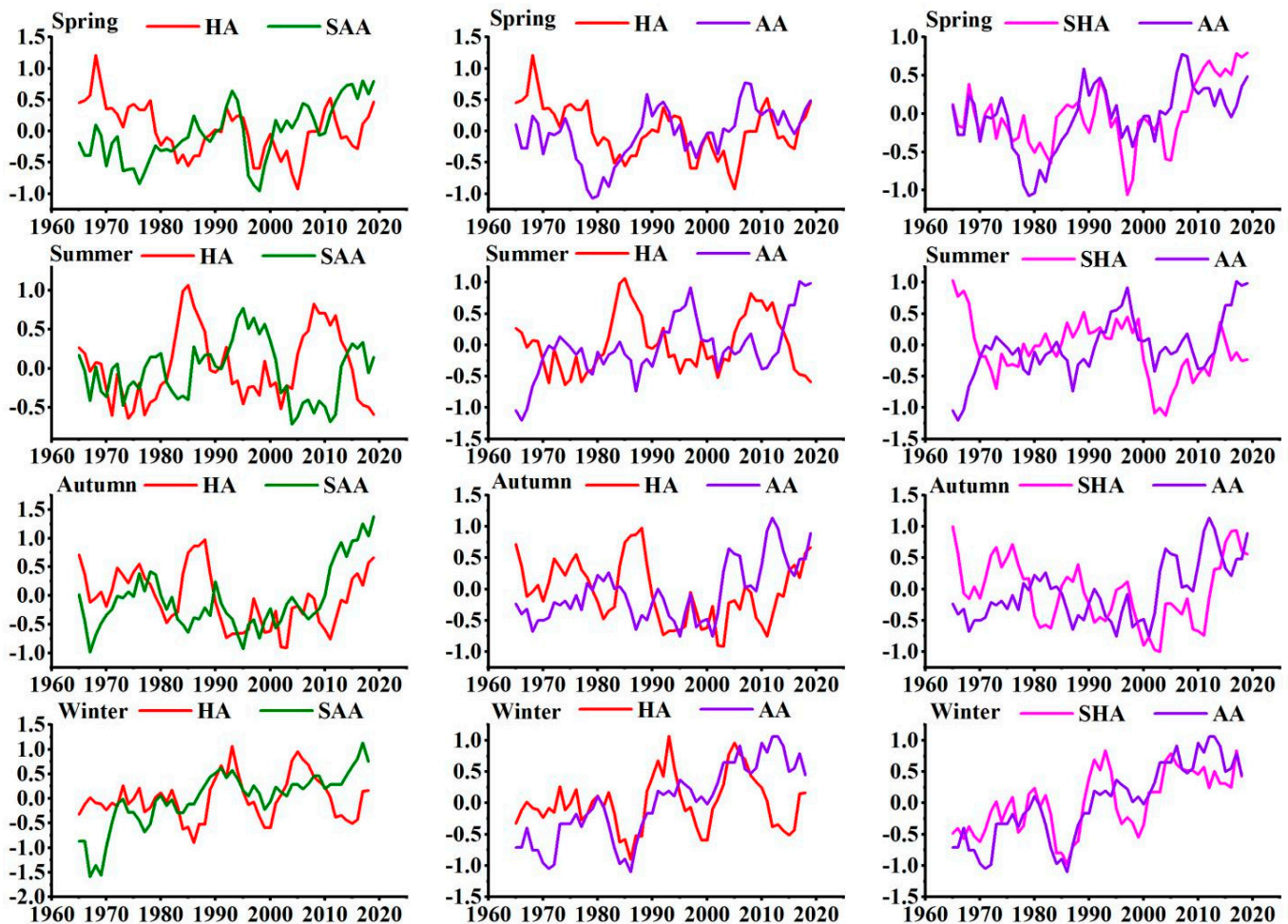


Figure 5. Five-year moving average of SPI3 in different seasons in dry-wet areas.

### 3.2. Evolution Characteristics of Drought Events

#### 3.2.1. Threshold Optimization

Selecting appropriate drought threshold can make our result of drought identification more accurate, so it is necessary to optimize the threshold. The maximum characteristic values of drought events identified by different thresholds were shown in Table 3.

**Table 3.** Comparison of maximum characteristic values of drought at different thresholds.

	Value (X1 = −0.3)	Time (X1 = −0.3)	Value (X1 = −0.4)	Time (X1 = −0.4)
MAX-DD(HA)	7	December 1981 to June 1982/April 1997 to October 1997/March 2001 to September 2001	7	April 1997 to October 1997
MAX-DS(HA)	8.66	March 2001 to September 2001	7.32	April 1997 to October 1997
MAX-DI(HA)	2.89	March 1962	2.89	March 1962
MAX-DD(SHA)	9	March 2001 to November 2001	9	March 2001 to November 2001
MAX-DS(SHA)	8.88	March 2001 to November 2001	8.88	March 2001 to November 2001
MAX-DI(SHA)	2.51	May 1979	2.51	May 1979
MAX-DD(SAA)	11	November 1964 to September 1965	11	November 1964 to September 1965
MAX-DS(SAA)	16.16	November 1964 to September 1965	16.16	November 1964 to September 1965
MAX-DI(SAA)	2.07	July 2015 to August 2015	2.07	July 2015 to August 2015
MAX-DD(AA)	12	November 1964 to September 1965	9	September 1974 to May 1975
MAX-DS(AA)	10.85	November 1964 to September 1965	8.97	February 1962 to August 1969
MAX-DI(AA)	2.42	April 1993	2.42	April 1993

Note: MAX-DD stands for maximum drought duration; MAX-DS stands for maximum drought severity; MAX-DI stands for maximum drought intensity.

As shown in Table 3, the identification results of  $X1 = -0.3$  and  $X1 = -0.4$  for the maximum characteristic values of drought events in the SHA and SAA were completely consistent, but different in the HA and AA. It can be seen that the drought events identified when  $X1 = -0.3$  had longer MAX-DD and MAX-DS, and had a better recognition effect on severe drought events in AA and HA. We verified two drought events in the HA, from April 1997 to October 1997 ( $X1 = -0.4$ ) and March 2001 to September 2001 ( $X1 = -0.3$ ). Firstly, the SPI12 in the HA in 1997 and 2001 were compared. It was found that the DS in the HA in 2001 ( $SPI12 = -2.09$ ) was more serious than that in 1997 ( $SPI12 = -1.87$ ). Secondly, the precipitation values corresponding to the two drought events were compared. It was found that the monthly average precipitation from July 1997 to October 1997 was 75.4 mm, and the monthly average precipitation from March 2001 to September 2001 was 71.8 mm. Therefore,  $X1 = -0.3$  was selected as the threshold of drought occurrence in the following drought event identification.

### 3.2.2. Spatial Distribution of Drought Characteristics

As shown in Figure 6, drought characteristics were quite different in space. The drought frequency (DF) was high in the east and low in the west, with the highest DF in the north of the SHA and the lowest DF in the south of the AA (Figure 6a); the average drought duration (ADD) showed a spatial distribution pattern of “one high and three low”. A high value area was distributed in the northwest of the AA, and three low value areas were distributed in the south of the AA, the north and south of the SAA (Figure 6b). There was no significant difference in the average drought severity (ADS) in HA, SHA and the SAA, while a clear north-south divergence is observed in AA: a high value center in the north and a large low value area in the south (Figure 6c). The average drought intensity (ADI) showed the spatial distribution characteristics of “two high and one low”. Two high value areas were located in the northern part of the AA and the southern part of the SHA and SAA, and a low value area was located in the southern part of the AA (Figure 6d).

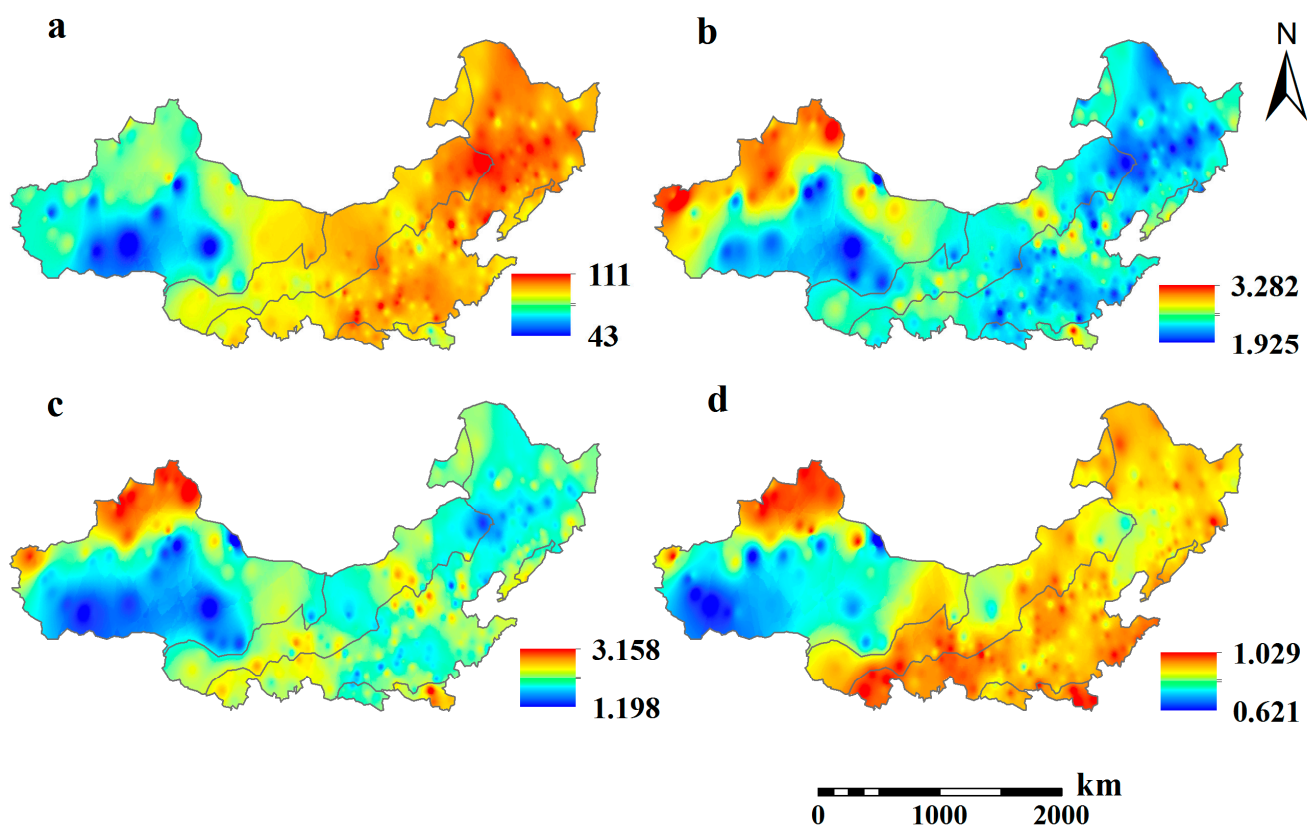


**Figure 6.** Spatial distribution of drought event characteristics (note: (a): drought frequency; (b): average drought duration; (c): average drought severity; (d): average drought intensity).

Overall, the south-central part of the AA was the low-value center of drought events; the DF and DI showed strong spatial consistency, and the DD and DS also showed good spatial consistency.

### 3.2.3. Change Trend of Drought Characteristics

As shown in Table 4, the DF of Northern China, SHA, SAA and AA all showed a decreasing trend, which was the most obvious in AA ( $-1.4857$  times/10a). The DF increased slightly only in HA ( $0.0571$  times/10a). The DD and DS of Northern China, SAA and AA showed a decreasing trend, which was the most obvious in SAA ( $-0.0104/10A$  and  $-0.108/10a$ ). The DD and DS of HA and SHA increased, but HA increased more than SHA. In both Northern China and all dry-wet areas, the DI showed a decreasing trend in the last 60 years, indicating that the DS of Northern China per unit time decreased. The analysis of drought characteristics revealed that drought decreased in Northern China but increased in HA and SHA.

**Table 4.** The change tendency rate of drought characteristic parameters.

	Northern China	HA	SHA	SAA	AA
DF (times/10a)	−0.4587	d	−1	−0.2286	−1.4857
DD	−0.0043/10a	0.0027/10a	0.0018/10a	−0.0104/10a	−0.007/10a
DS	−0.052/10a	0.019/10a	0.009/10a	−0.108/10a	−0.07/10a
DI	−0.011/10a	−0.012/10a	−0.0005/10a	−0.004/10a	−0.005/10a

## 4. Discussion

### 4.1. Influencing Factors of Meteorological Dry-Wet Changes in Different Seasons

As mentioned above, there were differences in meteorological dry-wet change characteristics in different seasons and areas in Northern China. The four dry-wet areas in winter and spring were mainly characterized by meteorological wetting, while the differences in summer and autumn were obvious. The HA and SHA with precipitation greater than 400 mm showed meteorological drying, while the SHA and AA with precipitation less than 400 mm showed meteorological wetting. The water balance of a region is largely affected by circulation factors. Through forewords analysis, we know that teleconnection factors such as the Arctic Oscillation (AO), ENSO (NINO3.4), North Pacific Decadal Oscillation (PDO) and North Atlantic Oscillation (NAO) can change the atmospheric circulation. Furthermore, the spatio-temporal changes of precipitation in different dry-wet areas are affected [3,23,49–51,53]. Therefore, the Pearson correlation coefficients of SPI and teleconnection indices (TP1, AO, NAO, WP, PNA, NINO3.4, AMO, SOI, PDO and APV) in different seasons were calculated in this paper to explore the effects of different circulation pattern systems on meteorological dry-wet changes in Northern China.

#### 4.1.1. Analysis on Influencing Factors of Meteorological Wetting in Winter and Spring

From Table 5, it could be seen that the winter meteorological wetting trend in Northern China was mainly positively influenced by TP1, AO, AMO and other factors. As a transitional season, spring was not only positively affected by TP1, AMO and PDO, but also negatively affected by SOI and APV.

**Table 5.** Correlation coefficients between winter and spring SPI3 and teleconnection index. Only significant values were shown (\*\*  $p$  value < 0.01).

	TP1	AO	AMO	SOI	PDO	APV
Winter	0.708 **	0.594 **	0.624 **	-	-	-
Spring	0.712 **	-	0.875 **	−0.376 **	0.468 **	−0.906 **

In winter, due to the strong radiation cooling effect, cold high is formed over the Qinghai-Tibet Plateau relative to the atmosphere at the same height and anticyclonic flow prevails, which intensifies winter wind. Then the cold air southward is enhanced, bringing abundant precipitation to Northern China. This effect will last until spring. AO is a “seesaw” phenomenon of pressure difference between the middle latitudes of the Northern Hemisphere and the Arctic region [73]. When experiencing AO+, the low pressure system in the Arctic region weakens while the high pressure system in the mid-latitude region strengthens, limiting the development of cold polar air to the mid-latitude region [74]. The weakening of the radial circulation system leads to the enhancement of the westerly circulation system. At the same time, AMO+ can heat the middle and upper troposphere of Eurasia [75] and enhance westerly wind fluctuations. Therefore, under the combined action of AO, AMO, PDO and TP1, winter in Northern China showed a trend of meteorological wetting.



As a transitional season, the meteorological wetting in spring is not only influenced by the continuous positive influence of TP1 and AMO, but also by the APV, which represents the intensity of the Asian polar vortex. When APV+, the southern force of the polar vortex is so strong that more precipitation is easy to form. However, at the same time, the weakening of APV fluctuations will reduce the interference of the radial circulation on the westerly circulation. Therefore, under the joint action of TP1, AMO, APV and other factors, Northern China also showed a trend of meteorological wetting in spring.

#### 4.1.2. Analysis of Influencing Factors of Summer and Autumn Dry-Wet Change

As mentioned above, the east became drying and the west became wetting in both summer and autumn (Figure 3). In summer, the main influencing factors of dry-wet changes in HA, SHA, SAA and AA were PNA, WP, PDO and TP1, respectively (Table 6). PNA represents the seesaw effect between the Aleutian low and the Hawaiian high. When PNA is in the positive (negative) phase, Hawaiian high is stronger (weaker). As part of the subtropical high, the strengthening (weakening) of the Hawaiian high will strengthen (weaken) the East Asian summer monsoon, thereby increasing (decreasing) precipitation over HA in summer. Therefore, the weakening fluctuation of PNA leads to the trend of meteorological drying in HA. Meanwhile, the enhanced fluctuation of NAO interferes greatly with the westerly wind, which is also one of the reasons for the meteorological drying in HA. Western Pacific Oscillation Index (WP) generally represents the phenomenon that the pressure of the western Pacific Ocean is high in the north and low in the south with 45° N as the boundary. When WP is in positive (negative) phase, the atmospheric pressure north of 45° N is higher (lower) than that south of 45° N, which weakens (strengthens) the East Asian summer monsoon to a certain extent, leading to less (more) precipitation in SHA. Thus, the enhanced fluctuation of WP leads to the trend of meteorological drying in SHA. In the meantime, the weakening of the East Asian summer monsoon due to the strengthening effect of the enhanced AMO fluctuations on the westerly wind is also one of the reasons for the drying of the SHA. In the meantime, the enhanced AMO fluctuation will weaken the East Asian summer monsoon caused by the strengthening effect of westerly wind, which is also one of the reasons for the drying of the SHA. The Pacific Decadal Oscillation (PDO) is a natural phenomenon of the inter-decade cycle of SST in the North Pacific Ocean. In the warm (cold) PDO phase, the SST over the central North Pacific is abnormally cold (warm), corresponding to the high (low) sea level pressure over the central Pacific. Therefore, the East Asian summer monsoon is strengthened (weakened), and the summer precipitation in the SAA (the eastern part of the SAA in this study belongs to the monsoon region and is affected by the East Asian summer monsoon) is increased (decreased). This is consistent with existing research conclusions [76]. Meanwhile, the strengthening of westerly wind fluctuation caused by the enhancement of AO fluctuation is also one of the reasons for the meteorological wetting in SAA. The influencing factors of meteorological wetting in AA in summer are relatively complex (Table 6), which is the result of the combined action of TP1, WP, NINO3.4, AMO, PDO and other factors. Among them, the enhanced fluctuation of TP1 in summer will intensify the convergence of the atmosphere in the middle troposphere of the northern Tibetan Plateau to the plateau surface, which in turn enhances the convective process of the near-surface atmosphere in the AA of northwest China. As a result, precipitation increases and AA shows a trend of meteorological wetting.



**Table 6.** Correlation coefficient between SPI3 and teleconnection index in summer. Only significant values were shown (\*\*  $p$  value < 0.01, \*  $p$  value < 0.05).

	HA	SHA	SAA	AA
TP1	-	−0.274 *	-	0.659 **
AO	-	-	0.351 **	-
NAO	−0.282 *	-	-	-
WP	-	−0.428 **	-	−0.61 **
PNA	0.381 **	-	-	-
NINO3.4	-	-	-	0.471 **
AMO	-	−0.342 *	-	0.348 **
SOI	-	-	-	−0.279 *
PDO	-	-	0.396 **	0.376 **

In autumn, the correlation between TP1 and SPI3 was the highest in HA and SHA, and both were negatively correlated, indicating that the enhancement of TP1 in autumn did not lead to the increase of precipitation in HA and SHA. The decrease in PDO fluctuation and the increase in WP and PNA fluctuation are the important factors of autumn meteorological drying in HA and SHA. AMO is the main influencing factor of dry-wet changes in SAA and AA (Table 7). The Atlantic Multiannual Oscillation Index (AMO) is a sea basin-scale SST anomaly with the multi-year variability that occurs in the North Atlantic region. It is a natural variability with a period of 65–80a and an amplitude of 0.4 °C [77]. AMO is significantly positively correlated with dry-wet changes in SAA and AA, which can be explained from the following two aspects. First, AMO strengthens the thermal difference between land and sea by heating the middle and upper troposphere of Eurasia [75]. Then, the East Asian summer monsoon is enhanced, which in turn affects the eastern part of the SAA. Thus, the precipitation in the SAA will increase. Second, the positive phase of the AMO heats up the Tibetan Plateau [78] and enhances the plateau monsoon, which in turn strengthens the convective processes in the AA of northwest China, resulting in an increase in precipitation.

**Table 7.** Correlation coefficient between SPI3 and teleconnection index in autumn. Only significant values were shown (\*\*  $p$  value < 0.01, \*  $p$  value < 0.05).

	HA	SHA	SAA	AA
TP1	−0.430 **	−0.444 **	−0.319 *	0.509 **
AO	-	-	0.356 **	-
WP	-	−0.277 *	-	-
PNA	-	−0.370 **	-	-
AMO	-	-	0.533 **	0.691 **
SOI	-	-	0.482 **	0.372 **
PDO	0.298 *	-	-	-

#### 4.1.3. Factors Influencing the Reverse Fluctuation of Meteorological Dry-Wet in HA and AA in Summer

According to Table 6, in summer, the teleconnection factors strongly correlated with HA meteorological drying were PNA and NAO, and the teleconnection factors strongly correlated with AA meteorological wetting were TPI, WP, NINO3.4, AMO, SOI and PDO. In order to further clarify the main reasons for the reverse fluctuation of meteorological dry-wet in HA and AA in summer, a comparative analysis was made between the above factors and the five-year moving average fluctuation process of SPI3 (Figure 7). In HA, SPI3 fluctuated in the same direction with NAO (Figure 7g), but in the opposite direction with PNA (Figure 8h). In AA, SPI3 fluctuated in the same direction with NINO3.4 and TP1 (Figure 7c,f), and in the opposite direction with AMO and SOI (Figure 7a,d,e), and had no consistent fluctuation relationship with WP and PDO (Figure 7b). The five-year moving average fluctuation process of each influence factor was shown in Figure 8. It can be seen

that the NAO had no consistent fluctuation relationship with TP1 and WP (Figure 8a,b), and was in the same direction with NINO3.4 and PDO (Figure 8c,f), and in the opposite direction with AMO and SOI (Figure 8d,e). There was no consistent fluctuation relationship between PNA and TP1 (Figure 8g), and PNA fluctuated in reverse with NINO3.4 and PDO (Figure 8i,l), and in the same direction with WP, AMO and SOI (Figure 8h,j,k). The above complex relationship can be visually demonstrated in Figure 9, and it can be found that the co-fluctuation of NAO-NINO3.4, PNA-AMO and PNA-SOI and the reverse fluctuation of NAO-SOI, NAO-AMO and PNA-NINO3.4 jointly determined the reverse fluctuation process (seesaw effect) of HA and AA in summer.

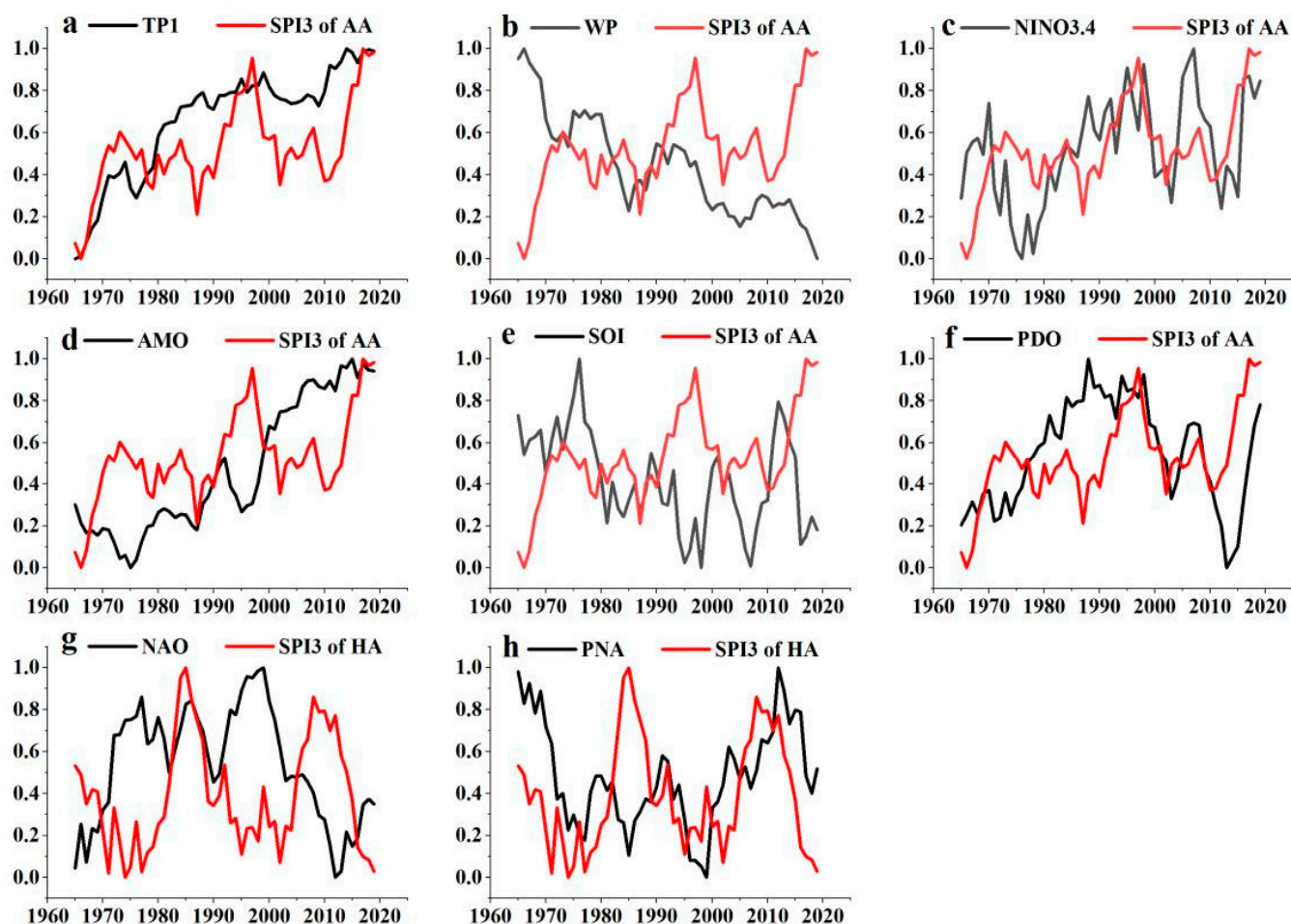


**Figure 7.** Five-year moving average of SPI3 and teleconnection index in HA and AA in summer (note: subfigure (a–f) shows the relationship between SPI3 of AA and the teleconnection index TP1, WP, NINO3.4, AMO, SOI and PDO, respectively; subfigure (g,h) shows the relationship between SPI3 of HA and the teleconnection index NAO and PNA, respectively).

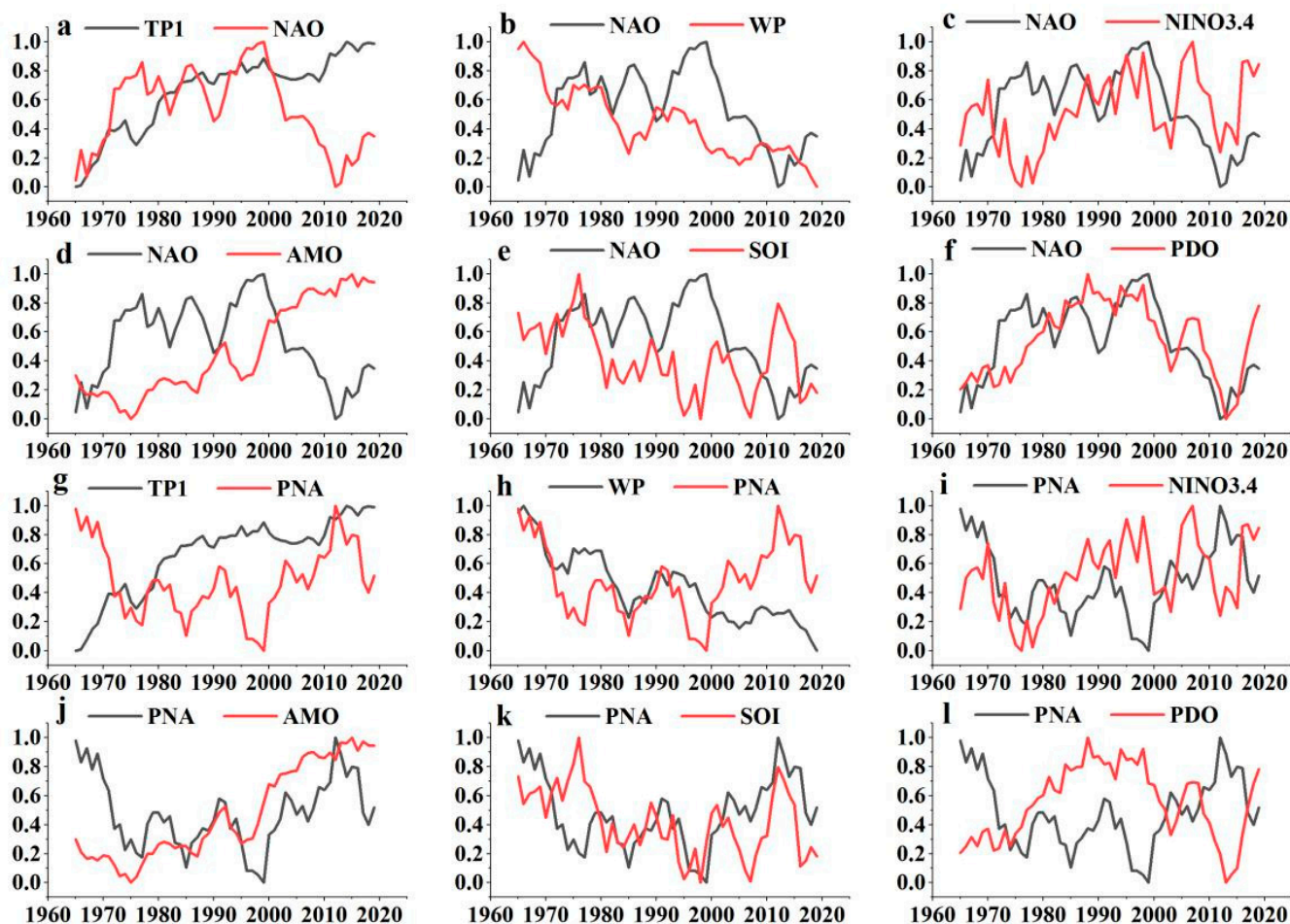


**Figure 8.** Five-year moving average of teleconnection factors (note: subfigure (a–f) show the relationship between NAO and TP1, WP, NINO3.4, AMO, SOI, and PDO; subfigure (g–l) show the relationship between PNA and TP1, WP, NINO3.4, AMO, SOI, and PDO).

#### 4.2. Comparison with Previous Studies and Future Prospect

In this paper, SPI was used to analyze the spatio-temporal change in meteorological dry-wet in Northern China in the last 60 years. In recent years, SPI has become increasingly important as a potential indicator of drought and can be compared across different precipitation regions [79,80]. In Northern China, there is a large east-west span and a large gap in precipitation. A direct comparison of precipitation changes at various stations cannot directly reflect the degree of dry-wet change. SPI is a very suitable index to reflect the dry-wet situation in Northern China. Due to differences in research scale and methods, our results were different from those of previous studies. For example, Tao et al. [60] used PDSI to find that the average duration of drought in semi-humid and semi-arid areas from 1982 to 2015 was longer and the intensity was larger. Our result is that the average duration of drought in Northern Xinjiang from 1960 to 2019 was longer and the intensity was larger. The influence of westerly circulation is greater in Northern Xinjiang, while the influence of the summer monsoon is greater in semi-humid and semi-arid areas. The precipitation fluctuation in the monsoon region is greater than that in the west wind region, and the atmosphere is more prone to disturbance and instability. Theoretically, the drought duration in the monsoon area should be shorter than that in the west wind area. Shi et al. [81] found that SPEI of about 74% regions in Northern China showed a decreasing trend from 1981 to 2017. This study found that SPI of 54.06% stations in Northern China showed an increasing trend from 1960 to 2019. This may be due to two factors. On the one hand, the time period studied was different, the summer monsoon changed from strong to weak in

the late 1970s [82], so the former results in a larger range of drying trend. On the other hand, the drought index considered different meteorological factors. The former took into account temperature, which led to a larger range of drying trend. Ren et al. [83] used SPEI to find that from 1959 to 2011, most areas in Northwest China showed a drying trend in spring, summer and autumn, and a wetting trend in winter. In this paper, it was found that most areas in Northwest China showed a wetting trend in all seasons from 1960 to 2019. On the one hand, it may be because the temperature was taken into account in the former, and the change in temperature had a great influence on the change trend of dry-wet. On the other hand, the trend of wetting in the 2010s had significantly changed the overall change trend. Zhuo et al. [58] used SPI to find that Northwest China was a region with a high incidence of drought disasters during 1961–2010. In this paper, it was found that drought events occurred more frequently in North China and Northeast China during 1960–2019. The precipitation in the monsoon region is unstable, and it is more prone to precipitation (negative) anomaly than in the non-monsoon region, and the occurrence frequency of drought is theoretically higher than that in the non-monsoon region. Although the research methods were different, we had come to the same or similar conclusions as our predecessors. For example, Han et al. [84] used the improved comprehensive meteorological drought index (MCI) to find that the frequency of drought in eastern China was higher than that in western China during 1960–2014, which is consistent with the conclusion that the frequency of drought events in North China and Northeast China was higher during 1960–2019. Zhang et al. [57] used the aridity index (AI) to find that drought in the monsoon fringe region during 1961–2013 was greatly affected by monsoon intensity. The earlier the northernmost of the monsoon fringe region appeared, the lower the latitude, the shorter the duration, and the drier the climate in the monsoon fringe region. In this study, we found that there was a drying trend in the monsoon fringe region from 1960 to 2019, which may be related to the weakening of summer monsoon [82]. In summary, our results are basically consistent with the facts and are reliable, indicating that SPI has good applicability to northern China. In addition, our results are similar to the results of dry-wet characteristics in the surrounding areas of TP. For example, Masoud Moradi [85] found that the drought in Kermanshah, Iran in recent decades has significantly decreased compared with the previous period. Firdos Khan [86] found that the precipitation of meteorological stations in the Karakoram region increased during 1962–1990. Jayanta Das [87] found that drought intensity was reduced in the western part of the Mud River Basin in Rajasthan, western India. At the same time, this paper discussed the influence factors of dry-wet changes in different seasons in different dry-wet areas by using teleconnection factors, which can provide important references for drought disaster prevention and mitigation in Northern China and the establishment of drought monitoring and early warning system. However, due to the research scale of this paper, the influence factors of meteorological dry-wet were discussed only from the large circulation pattern, and the influence factors of local dry-wet change were lacking in the discussion. Future research should pay more attention to the local area, and consider a variety of local influencing factors, such as water resources conditions, human activities, geological landforms, relative humidity, wind speed and solar radiation.



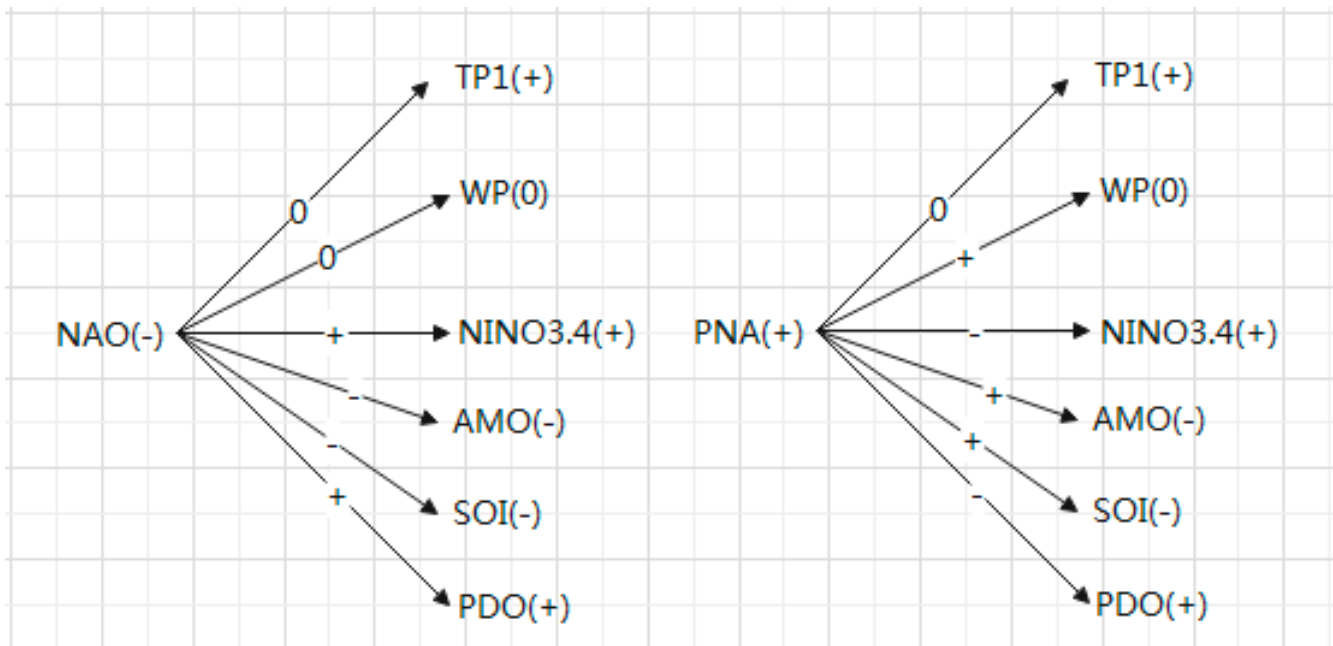


**Figure 9.** Wave logic of teleconnection factors (note: the symbol in parentheses is the fluctuation relation between the teleconnection factors and SPI3 of the dry-wet area, the symbol on the arrow is the relationship between teleconnection factors, “+” means forward fluctuation, “-” means reverse fluctuation, and “0” means no consistent fluctuation).

## 5. Conclusions

Based on the standardized precipitation index (SPI), Mann-Kendall method (MK) and Sen Slope, the dry-wet changes and drought evolution characteristics in Northern China from 1960 to 2019 were studied. Pearson correlation was used to analyze the relationship between dry-wet changes and teleconnection correlation factors and reveal the driving mechanism of dry-wet change in each dry-wet area. The main conclusions were as follows:

- (1) At the inter-annual scale, the number of wetting stations in Northern China was slightly more than that of drying stations. It presented the spatio-temporal characteristics of drying in the HA and SHA in the east, and wetting in the SAA and AA in the west. The AA and SAA in the west had the same trend of wetting at the inter-annual and seasonal scales, while the HA and SHA in the east had complex meteorological dry-wet changes in different seasons. The AA and HA not only showed the opposite dry-wet trend, but also appeared a very pronounced “reverse fluctuation” called the “seesaw effect” in summer.
- (2) The drought characteristics differed widely in space. Overall, the south-central part of the AA was the low-value center of drought events; the DF and DI showed strong spatial consistency, as did the DD and DS in space. From 1960 to 2019, the DF in the SHA, SAA and AA showed a decreasing trend. The DD and DS of SHA and AA showed a decreasing trend, while HA and SHA increased. In addition, the DI of each dry-wet area showed a decreasing trend.
- (3) TP1 ( $r = 0.708$ ,  $p = 0.01$ ) and APV ( $r = -0.906$ ,  $p = 0.01$ ) were the main influencing factors of dry-wet change in winter and spring in Northern China, respectively. In summer, PNA, WP, PDO and TP1 were the main influencing factors of dry-wet change in HA, SHA, SAA and AA, respectively. In autumn, TP1 was the main influencing factor of dry-wet change in HA and SHA, while AMO was the main influencing factor of that in SAA and AA. Moreover, the co-direction fluctuation of NAO-NINO3.4, PNA-AMO and PNA-SOI and the reverse fluctuation of NAO-SOI, NAO-AMO and PNA-NINO3.4 jointly determined the reverse fluctuation process of SPI3 of HA and AA in summer.

**Author Contributions:** Conceptualization, J.Z.; Methodology, Y.Q., Z.G., C.L. (Chuyu Luo) and X.W.; Software, W.S., D.Z. and C.W.; Formal analysis, H.T.; Data curation, H.T. and Y.Q.; Writing—original draft, H.T.; Writing—review & editing, J.Z., H.T. and Y.Q.; Supervision, J.Z.; Funding acquisition, X.Y., C.L. (Chunfang Liu) and W.W. All authors have read and agreed to the published version of the manuscript.

**Funding:** This research was funded by the National Natural Science Foundation of China grant number 41761047, 41861034, 41861040 and 32060373.

**Institutional Review Board Statement:** Not applicable.

**Informed Consent Statement:** Informed consent was obtained from all subjects involved in the study.

**Data Availability Statement:** The data used in this study are available at <http://data.cma.cn>, <http://www.noaa.gov/> and <http://cmdp.ncc.cma.gov.cn> (accessed on 31 October 2020).

**Acknowledgments:** We would like to thank the colleagues in the Northwest Normal University for its help in the writing process. We are grateful to the anonymous reviewers and editorial staff for their constructive and helpful suggestions.

**Conflicts of Interest:** The authors declare no conflict of interest.

## References

1. Wang, J.S.; Li, Y.H.; Wang, R.Y.; Feng, J.Y.; Zhao, Y.X. Preliminary analysis on the demand and review of progress in the field of meteorological drought research. *J. Arid Meteorol.* **2012**, *30*, 497–508.
2. Zargar, A.; Sadiq, R.; Naser, B.; Khan, F.I. A review of drought indices. *Environ. Rev.* **2011**, *19*, 333–349. [[CrossRef](#)]
3. Wang, H.; Chen, Y.; Pan, Y.; Li, W. Spatial and temporal variability of drought in the arid region of China and its relationships to teleconnection indices. *J. Hydrol.* **2015**, *523*, 283–296. [[CrossRef](#)]
4. Vicente-Serrano, S.M.; Beguería, S.; López-Moreno, J.I. A multiscalar drought index sensitive to global warming: The standardized precipitation evapotranspiration index. *J. Clim.* **2010**, *23*, 1696–1718. [[CrossRef](#)]
5. Mishra, A.K.; Singh, V.P. Drought modeling—A review. *J. Hydrol.* **2011**, *403*, 157–175. [[CrossRef](#)]
6. Touma, D.; Ashfaq, M.; Nayak, M.A.; Kao, S.-C.; Diffenbaugh, N.S. A multi-model and multi-index evaluation of drought characteristics in the 21st century. *J. Hydrol.* **2015**, *526*, 196–207. [[CrossRef](#)]
7. AghaKouchak, A.; Feldman, D.; Hoerling, M.; Huxman, T.; Lund, J. Water and climate: Recognize anthropogenic drought. *Nature* **2015**, *524*, 409–411. [[CrossRef](#)]
8. Zhang, B.; He, C. A modified water demand estimation method for drought identification over arid and semiarid regions. *Agric. For. Meteorol.* **2016**, *230*, 58–66. [[CrossRef](#)]
9. Frank, A.; Armenski, T.; Gocic, M.; Popov, S.; Popovic, L.; Trajkovic, S. Influence of mathematical and physical background of drought indices on their complementarity and drought recognition ability. *Atmospheric Res.* **2017**, *194*, 268–280. [[CrossRef](#)]
10. Frich, P.; Alexander, L.; Della-Marta, P.; Gleason, B.; Haylock, M.; Tank, A.K.; Peterson, T. Observed coherent changes in climatic extremes during the second half of the twentieth century. *Clim. Res.* **2002**, *19*, 193–212. [[CrossRef](#)]
11. Wang, L.; Chen, W. Applicability analysis of standardized precipitation evapotranspiration index in drought monitoring in China. *Plateau Meteorol.* **2014**, *33*, 423–431. (In Chinese)
12. Hoerling, M.; Eischeid, J.; Kumar, A.; Leung, R.; Mariotti, A.; Mo, K.; Schubert, S.; Seager, R. Causes and Predictability of the 2012 Great Plains Drought. *Bull. Am. Meteor. Soc.* **2014**, *95*, 269–282. [[CrossRef](#)]
13. He, P.; Ma, X.; Sun, Z.; Han, Z.; Ma, S.; Meng, X. Compound drought constrains gross primary productivity in Chinese grasslands. *Environ. Res. Lett.* **2022**, *17*, 104054. [[CrossRef](#)]
14. Lei, T.; Pang, Z.; Wang, X.; Li, L.; Fu, J.; Kan, G.; Zhang, X.; Ding, L.; Li, J.; Huang, S.; et al. Drought and Carbon Cycling of Grassland Ecosystems under Global Change: A Review. *Water* **2016**, *8*, 460. [[CrossRef](#)]
15. Schubert, S.D.; Stewart, R.E.; Wang, H.; Barlow, M.; Berbery, E.H.; Cai, W.; Hoerling, M.P.; Kanikicharla, K.K.; Koster, R.D.; Lyon, B.; et al. Global meteorological drought: A synthesis of current understanding with a focus on sst drivers of precipitation deficits. *J. Clim.* **2016**, *29*, 3989–4019. [[CrossRef](#)]
16. Lesk, C.; Rowhani, P.; Ramankutty, N. Influence of extreme weather disasters on global crop production. *Nature* **2016**, *529*, 84–87. [[CrossRef](#)] [[PubMed](#)]
17. Igbawua, T.; Zhang, J.; Yao, F.; Zhang, D. Assessment of moisture budget over West Africa using MERRA-2's aerological model and satellite data. *Clim. Dyn.* **2019**, *52*, 83–106. [[CrossRef](#)]
18. Yao, N.; Li, Y.; Lei, T.; Peng, L. Drought evolution, severity and trends in mainland China over 1961. *Sci. Total Environ.* **2018**, *616*, 73–89. [[CrossRef](#)]
19. Liu, Q.; Zhang, S.; Zhang, H.; Bai, Y.; Zhang, J. Monitoring drought using composite drought indices based on remote sensing. *Sci. Total Environ.* **2020**, *711*, 134585. [[CrossRef](#)]



20. Depsky, N.; Pons, D. Meteorological droughts are projected to worsen in Central America's dry corridor throughout the 21st century. *Environ. Res. Lett.* **2020**, *16*, 014001. [[CrossRef](#)]
21. Coelho Junior, L.M.; de Lourdes da Costa Martins, K.; Carvalho, M. Carbon footprint associated with firewood consumption in northeast Brazil: An analysis by the IPCC 2013 GWP 100y Criterion. *Waste Biomass Valorization* **2019**, *10*, 2985–2993. [[CrossRef](#)]
22. Sharma, J.; Ravindranath, N.H. Applying IPCC 2014 framework for hazard-specific vulnerability assessment under climate change. *Environ. Res. Commun.* **2019**, *1*, 051004. [[CrossRef](#)]
23. Wang, F.; Wang, Z.; Yang, H.; Di, D.; Zhao, Y.; Liang, Q. Utilizing GRACE-based groundwater drought index for drought characterization and teleconnection factors analysis in the North China Plain. *J. Hydrol.* **2020**, *585*, 124849. [[CrossRef](#)]
24. Yuan, W.; Zhou, G. Theoretical Study and Research Prospect on Drought Indices. *Adv. Earth Sci.* **2004**, *6*, 982–991.
25. Wu, Y.; Bake, B.; Zhang, J.; Rasulov, H. Spatio-temporal patterns of drought in North Xinjiang, China, 1961–2012 based on meteorological drought index. *J. Arid. Land* **2015**, *7*, 527–543. [[CrossRef](#)]
26. Karabulut, M. Drought analysis in Antakya-Kahramanmaraş Graben, Turkey. *J. Arid Land* **2015**, *7*, 741–754. [[CrossRef](#)]
27. Palmer, W.C. *Keeping Track of Crop Moisture Conditions, Nationwide: The New Crop Moisture Index*; Taylor & Francis: Abingdon, UK, 1968; Volume 1, pp. 156–161.
28. McKee, T.B.; Doesken, N.J.; Kleist, J. The relationship of drought frequency and duration to time scales. In Proceedings of the Eighth Conference on Applied Climatology, Anaheim, CA, USA, 17–22 January 1993; pp. 179–183.
29. Wu, M.; Li, Y.; Hu, W.; Yao, N.; Li, L.; Liu, D.L. Spatiotemporal variability of standardized precipitation evapotranspiration index in mainland China over 1961–2016. *Int. J. Clim.* **2020**, *40*, 4781–4799. [[CrossRef](#)]
30. Christos, A.K.; Stavros, A.; Demetrios, E.T.; George, A. Application of the Standardized Precipitation Index (SPI) in Greece. *Water* **2011**, *3*, 787–805.
31. Karavitis, C.A.; Skondras, N.A.; Tsesmelis, D.E.; Stamatakos, C.G.; Alexandris, S.G.; Fassouli, V.P. Drought impacts archive and drought vulnerability index. *DMCSEE Summ. Proj. Result* **2012**.
32. Karavitis, C.A.; Skondras, N.A.; Tsesmelis, D.E.; Stamatakos, C.G.; Alexandris, S.G.; Fassouli, V.P. Linking drought characteristics to impacts on a spatial and temporal scale. *Water Policy* **2014**, *16*, 1172–1197. [[CrossRef](#)]
33. Tsesmelis, D.E.; Oikonomou, P.D.; Vasilakou, C.G.; Skondras, N.A.; Fassouli, V.; Alexandris, S.G.; Grigg, N.S.; Karavitis, C.A. Assessing structural uncertainty caused by different weighting methods on the Standardized Drought Vulnerability Index (SDVI). *Stoch. Environ. Res. Risk Assess.* **2019**, *33*, 515–533. [[CrossRef](#)]
34. Kalisa, W.; Zhang, J.; Igbawua, T.; Ujoh, F.; Ebohon, O.J.; Namugize, J.N.; Yao, F. Spatio-temporal analysis of drought and return periods over the East African region using Standardized Precipitation Index from 1920 to 2016. *Agric. Water Manag.* **2020**, *237*, 106195. [[CrossRef](#)]
35. Achour, K.; Meddi, M.; Zeroual, A.; Bouabdelli, S.; Maccioni, P.; Moramarco, T. Spatio-temporal analysis and forecasting of drought in the plains of northwestern Algeria using the standardized precipitation index. *J. Earth Syst. Sci.* **2020**, *129*, 1–22. [[CrossRef](#)]
36. Razi, T. Performance evaluation of different probability distribution functions for computing Standardized Precipitation Index over diverse climates of Iran. *Int. J. Clim.* **2021**, *41*, 3352–3373. [[CrossRef](#)]
37. Song, Z.; Xia, J.; She, D.; Zhang, L.; Hu, C.; Zhao, L. The development of a Nonstationary Standardized Precipitation Index using climate covariates: A case study in the middle and lower reaches of Yangtze River Basin, China. *J. Hydrol.* **2020**, *588*, 125115. [[CrossRef](#)]
38. Oliveira Júnior, J.F.; Gois, G.; Silva, I.J.L.; Jardim, A.M.R.F.; Silva, M.V.; Shah, M.; Jamjareegulgarn, P. Wet and dry periods in the state of Alagoas (Northeast Brazil) via Standardized Precipitation Index. *J. Atmos. Sol. Terr. Phys.* **2021**, *224*, 105746. [[CrossRef](#)]
39. Abdelmalek, M.B.; Nouiri, I. Study of trends and mapping of drought events in Tunisia and their impacts on agricultural production. *Sci. Total Environ.* **2020**, *734*, 139311. [[CrossRef](#)]
40. Baronetti, A.; González-Hidalgo, J.C.; Vicente-Serrano, S.M.; Acquafredda, F.; Fratianni, S. A weekly spatio-temporal distribution of drought events over the Po Plain (North Italy) in the last five decades. *Int. J. Climatol.* **2020**, *40*, 4463–4476. [[CrossRef](#)]
41. Ayala, J.H.; Heslar, M. Examining the spatiotemporal characteristics of droughts in the Caribbean using the standardized precipitation index (SPI). *Clim. Res.* **2019**, *78*, 103–116. [[CrossRef](#)]
42. Yuan, N.; Yang, Q.; Liu, J.; Tao, L.; Feng, J.M.; Ma, Z.G. Research progress on attribution and prediction of interdecadal climate events. *China Basic Sci.* **2019**, *21*, 36–44.
43. Dai, A.; Fyfe, J.C.; Xie, S.-P.; Dai, X. Decadal modulation of global surface temperature by internal climate variability. *Nat. Clim. Chang.* **2015**, *5*, 555–559. [[CrossRef](#)]
44. Gu, G.; Adler, R.F. Spatial Patterns of Global Precipitation Change and Variability during 1901–2010. *J. Clim.* **2015**, *28*, 4431–4453. [[CrossRef](#)]
45. Gu, G.; Adler, R.F.; Huffman, G. Long-term changes/trends in surface temperature and precipitation during the satellite era (1979–2012). *Clim. Dyn.* **2015**, *46*, 1091–1105. [[CrossRef](#)]
46. Yang, Q.; Ma, Z.; Fan, X.; Yang, Z.-L.; Xu, Z.; Wu, P. Decadal Modulation of Precipitation Patterns over Eastern China by Sea Surface Temperature Anomalies. *J. Clim.* **2017**, *30*, 7017–7033. [[CrossRef](#)]
47. Yang, Q.; Ma, Z.; Xu, B. Modulation of monthly precipitation patterns over East China by the Pacific Decadal Oscillation. *Clim. Chang.* **2016**, *144*, 405–417. [[CrossRef](#)]

48. Ma, F.; Ye, A.; You, J.; Duan, Q. 2015–2016 floods and droughts in China, and its response to the strong El Niño. *Sci. Total Environ.* **2018**, *627*, 1473–1484. [[CrossRef](#)]
49. Nalley, D.; Adamowski, J.; Biswas, A.; Gharabaghi, B.; Hu, W. A multiscale and multivariate analysis of precipitation and streamflow variability in relation to ENSO, NAO and PDO. *J. Hydrol.* **2019**, *574*, 288–307. [[CrossRef](#)]
50. Allen, R.J.; Luptowitz, R. El Niño-like Teleconnection Increases California Precipitation in Response to Warming. *Nat. Commun.* **2017**, *8*, 16055. [[CrossRef](#)]
51. Casanueva, A.; Rodríguez-Puebla, C.; Frías, M.D.; González-Reviriego, N. Variability of extreme precipitation over Europe and its relationships with teleconnection patterns. *Hydrol. Earth Syst. Sci.* **2014**, *18*, 709–725. [[CrossRef](#)]
52. Wang, L.N.; Zhu, Q.K.; Zhao, W.J.; Zhao, X.K. The drought trend and its relationship with rainfall intensity in the Loess Plateau of China. *Nat. Hazard* **2015**, *77*, 479–495. [[CrossRef](#)]
53. Zhang, L.L.; Zhou, J.J.; Zhang, H.W.; Wang, B.; Cao, J.J. Temporal and spatial patterns of climate drought-wet and drought event based on Standard Precipitation Index in Shiyang River Basin. *Acta Ecol. Sin.* **2017**, *37*, 996–1007.
54. Hu, Z.; Zhou, J.; Zhang, L.; Wei, W. Climate dry-wet change and drought evolution characteristics of different dry-wet areas in northern China. *Acta Ecologica Sinica.* **2018**, *38*, 1908–1919.
55. Ribeiro, A.S.; Almeida, M.C.; Cox, M.G.; Sousa, J.A.; Martins, L.; Loureiro, D.; Brito, R.; Silva, M.; Soares, A.C. Role of measurement uncertainty in the comparison of average areal rainfall methods. *Metrologia.* **2021**, *58*, 044001. [[CrossRef](#)]
56. Zhou, J.; Li, Q.; Wang, L.; Lei, L.; Huang, M.; Xiang, J.; Feng, W.; Zhao, Y.; Xue, D.; Liu, C.; et al. Impact of Climate Change and Land-Use on the Propagation from Meteorological Drought to Hydrological Drought in the Eastern Qilian Mountains. *Water* **2019**, *11*, 1602. [[CrossRef](#)]
57. Zhang, H.; Zhang, Q. Chinese Meteorological Society. In Proceedings of the 33rd Annual Meeting of Chinese Meteorological Society, Xi'an, China, 2 November 2016.
58. Zhuo, Y.; Bao, Y.M.; Liu, G.X.; Yu, F.M. Characteristics of Drought Disaster Frequency of China in Last 50 Years Based on the Drought Index SPI. In *Information Technology in Risk Analysis and Crisis Response, Proceedings of the 6th Annual Conference of Risk Analysis Committee of China Disaster Prevention Association, Hohhot, China, 23 August 2014*; Risk Analysis Committee of China Disaster Prevention Association: Beijing, China, 2014; pp. 859–863.
59. Chen, Z.Q.; Hou, W.; Zuo, D.D.; Hu, J.G. Research on Drought Characteristics in China Based on the Revised Copula Function. *J. Arid. Meteorol.* **2016**, *34*, 213–222.
60. Tao, R.; Zhang, K. PDSI-based analysis of characteristics and spatiotemporal changes of meteorological drought in China from 1982 to 2015. *Water Resour. Prot.* **2020**, *426*, 50–56.
61. Wang, X.F.; Zhang, Y.; Feng, X.M.; Feng, Y.; Xue, Y.Y.; Pan, N.Q. Analysis and application of drought characteristics based on run theory and Copula function. *Trans. Chin. Soc. Agric. Eng.* **2017**, *33*, 206–214. (In Chinese)
62. Liu, X.; Leng, X.; Sun, G.; Peng, Y.; Huang, Y.; Yang, Q. Assessment of drought characteristics in Yunnan Province based on SPI and SPEI from 1961 to 2100. *Trans. Chin. Soc. Agric. Mach.* **2018**, *49*, 299.
63. Li, M.; Hu, W.; Wang, G.; Chai, X.; Zhang, L. Drought Risk in Monsoon Area of the Eastern China Based on Copula Function. *Sci. Geogr. Sinica* **2019**, *39*, 506–515.
64. Ma, J.; Liu, B.; Xia, J. Analysis of Temporal and Spatial Characteristics of Meteorological Drought in Shandong Province Based on the Theory of Runs. *Yellow River.* **2013**, *35*, 4–7.
65. Mann, H.B. Nonparametric tests against trend. *Econom. J. Econom. Soc.* **1945**, *13*, 245–259. [[CrossRef](#)]
66. Kendall, M.G. *Rank Correlation Measures*; Charles Griffin: London, UK, 1975; p. 220.
67. Liu, C.; Yang, C.; Yang, Q.; Wang, J. Spatiotemporal drought analysis by the standardized precipitation index (SPI) and standardized precipitation evapotranspiration index (SPEI) in Sichuan Province, China. *Sci. Rep.* **2021**, *11*, 1–14. [[CrossRef](#)] [[PubMed](#)]
68. Jain, S.K.; Kumar, V. Trend analysis of rainfall and temperature data for India. *Curr. Sci. India* **2012**, *102*, 37–49.
69. Raj, P.P.N.; Azeez, P.A. Trend analysis of rainfall in Bharathapuzha River basin, Kerala, India. *Int. J. Climatol.* **2012**, *32*, 533–539.
70. Lettenmaier, D.P.; Wood, E.F.; Wallis, J.R. Hydro-climatological trends in the continental United-States, 1948–1988. *J. Clim.* **1994**, *7*, 586–607. [[CrossRef](#)]
71. Asadi Zarch, M.A.; Sivakumar, B.; Sharma, A. Droughts in a warming climate: A global assessment of Standardized precipitation index (SPI) and Reconnaissance drought index (RDI). *J. Hydrol.* **2015**, *526*, 183–195. [[CrossRef](#)]
72. Leng, G.; Hall, J. Crop yield sensitivity of global major agricultural countries to droughts and the projected changes in the future. *Sci. Total Environ.* **2019**, *654*, 811–821. [[CrossRef](#)]
73. Thompson, D.W.; Wallace, J.M. The Arctic Oscillation signature in the wintertime geopotential height and temperature fields. *Geophys. Res. Lett.* **1998**, *25*, 1297–1300. [[CrossRef](#)]
74. Wen, S.; Zhou, J.; Hu, M. The Linkage between Winter-spring Arctic Oscillation and Precipitation over Western and Central China. *J. Chengdu Univ. Inf. Technol.* **2019**, *34*, 403–410.
75. Wang, Y.; Li, S.; Luo, D. Seasonal response of Asian monsoonal climate to the Atlantic Multidecadal Oscillation. *J. Geophys. Res. Atmos.* **2009**, *114*. [[CrossRef](#)]
76. Jia, Y.Q.; Zhang, B. Relationship of Dry-Wet Climate Changes in Northern China in the Past 57 Years with Pacific Decadal Oscillation (PDO). *Acta Ecol. Sin.* **2019**, *56*, 1085–1097.
77. Kerr, R.A. A North Atlantic climate pacemaker for the centuries. *Science* **2000**, *288*, 1984–1985. [[CrossRef](#)] [[PubMed](#)]

78. Feng, S.; Hu, Q. How the North Atlantic Multidecadal Oscillation may have influenced the Indian summer monsoon during the past two millennia. *Geophys. Res. Lett.* **2008**, *35*. [[CrossRef](#)]
79. Kumar, M.N.; Murthy, C.S.; Sai, M.V.R.S.; Roy, P.S. On the use of Standardized Precipitation Index (SPI) for drought intensity assessment. *Meteorol. Appl.* **2009**, *16*, 381–389. [[CrossRef](#)]
80. Solanki, J.K.; Parekh, F. Drought assessment using standardized precipitation index. *Int. J. Sci. Res.* **2014**, *3*, 1073–1076.
81. Shi, S.; Wang, F.; Jin, K.; Ding, W. Temporal and spatial characteristics of drought based on SPEI in northern China from 1981 to 2017. *Agric. Res. Arid Areas* **2019**, *37*, 215–222.
82. Ma, Z.; Fu, Z. Basic facts of aridity in northern China from 1951 to 2004. *Chin. Sci. Bull.* **2006**, *51*, 2429–2439. [[CrossRef](#)]
83. Ren, P.; Zhang, B.; Zhang, T.; Li, X.Y.; Chen, L.; Lu, L.P. Trend analysis of meteorological drought change in Northwest China on standardized precipitation evapotranspiration index. *Bull. Soil Water Conserv.* **2014**, *34*, 182–187.
84. Han, L.; Zhang, Q.; Jia, J.; Wang, Y.; Huang, T. Drought severity, frequency, duration and regional differences in China. *J. Des. Res.* **2019**, *39*, 1–10.
85. Moradi, M.; Yahya Safari, S.; Biglari, H.; Ghayebzadeh, M.; Darvishmotevalli, M. Multi-year assessment of drought changes in the Kermanshah city by standardized precipitation index. *Int. J. Power* **2016**, *8*, 17975–17987.
86. Khan, F.; Ali, S.; Mayer, C.; Ullah, H.; Muhammad, S. Climate change and spatio-temporal trend analysis of climate extremes in the homogeneous climatic zones of Pakistan during 1962–2019. *PLoS ONE* **2022**, *17*, e0271626. [[CrossRef](#)] [[PubMed](#)]
87. Das, J.; Gayen, A.; Saha, P.; Bhattacharya, S.K. Meteorological drought analysis using Standardized Precipitation Index over Luni River Basin in Rajasthan, India. *SN Appl. Sci.* **2020**, *2*, 1–17. [[CrossRef](#)]

**Disclaimer/Publisher’s Note:** The statements, opinions and data contained in all publications are solely those of the individual author(s) and contributor(s) and not of MDPI and/or the editor(s). MDPI and/or the editor(s) disclaim responsibility for any injury to people or property resulting from any ideas, methods, instructions or products referred to in the content.